Climate signatures on lake and wetland size distributions in arctic deltas

Lawrence Vulis[1], Alejandro Tejedor[2], Ilya Zaliapin[3], Joel Carey Rowland[4], and Efi Foufoula-Georgiou[1]

[1]University of California, Irvine
[2]Paris-Sorbonne University Abu Dhabi
[3]University of Nevada Reno
[4]Los Alamos National Laboratory (DOE)

November 24, 2022

Abstract

Understanding how thermokarst lakes on arctic river deltas will respond to rapid warming is critical for projecting how carbon storage and fluxes will change in those vulnerable environments. Yet, this understanding is currently limited partly due to the complexity of disentangling significant interannual variability from the longer-term surface water signatures on the landscape, using the summertime window of optical spaceborne observations. Here, we rigorously separate perennial lakes from ephemeral wetlands on 12 arctic deltas and report distinct size distributions and climate trends for the two waterbodies. Namely, we find a lognormal distribution for lakes and a power-law distribution for wetlands, consistent with a simple proportionate growth model and inundated fractal topography, respectively. Furthermore, while no trend with temperature is found for wetlands, a statistically significant decreasing trend of mean lake size with warmer temperatures is found, attributed to colder deltas having deeper and thicker permafrost preserving larger lakes.

Climate signatures on lake and wetland size distributions in arctic deltas

Lawrence Vulis[1*], Alejandro Tejedor[2,1], Ilya Zaliapin[3], Joel C. Rowland[4], and Efi Foufoula-Georgiou[1,5]

[1]Department of Civil and Environmental Engineering, University of California Irvine, lvulis@uci.edu
[2]Department of Science and Engineering, Sorbonne University Abu Dhabi
[3]Department of Mathematics and Statistics, University of Nevada Reno
[4]Earth and Environmental Sciences Division, Los Alamos National Laboratory
[5]Department of Earth System Science, University of California Irvine

Key Points:

1. Lake areas in arctic deltas exhibit a lognormal distribution associated with a simple mechanistic growth process.
2. Wetland areas exhibit a power law distribution consistent with inundated fractal topography.
3. Colder arctic deltas have larger average lake sizes, likely due to thicker permafrost restricting sub-lake hydrologic connectivity.

ABSTRACT

Understanding how thermokarst lakes on arctic river deltas will respond to rapid warming is critical for projecting how carbon storage and fluxes will change in those vulnerable environments. Yet, this understanding is currently limited partly due to the complexity of disentangling significant interannual variability from the longer-term surface water signatures on the landscape, using the summertime window of optical spaceborne observations. Here, we rigorously separate perennial lakes from ephemeral wetlands on 12 arctic deltas and report distinct size distributions and climate trends for the two waterbodies. Namely, we find a lognormal distribution for lakes and a power-law distribution for wetlands, consistent with a simple proportionate growth model and inundated fractal topography, respectively. Furthermore, while no trend with temperature is found for wetlands, a statistically significant decreasing trend of mean lake size with warmer temperatures is found, attributed to colder deltas having deeper and thicker permafrost preserving larger lakes.

Plain Language Summary

Arctic river deltas are landscapes facing significant risk from climate change, in part due to their unique permafrost features. In particular, thermokarst lakes in ice-rich permafrost are expected to both expand and drain under warming-induced permafrost thaw, reconfiguring deltaic hydrology and impacting the arctic carbon cycle. A limitation in understanding how thermokarst lake cover might be changing, is the significant interannual variability in water cover in flat regions such as deltas, which makes it difficult to distinguish between perennially inundated, thermally relevant waterbodies, and ephemerally inundated waterbodies. Here, we present a pan-Arctic study of 12 arctic deltas wherein we classify observed waterbodies into perennial lakes and ephemeral wetlands capitalizing on the historical record of remote sensing data. We provide evidence that thermokarst lake sizes are universally lognormally distributed and that historical temperature trends are encoded in lake sizes, while wetland sizes are power law distributed and have no temperature trend. These findings pave the way for quantitative insight into lake cover changes on arctic deltas and associated carbon and hydrologic cycle impacts under future climate change.

1. Introduction

Coastal river deltas are landscapes at significant risk from sea level rise and sediment deprivation (Nienhuis et al., 2020; Syvitski et al., 2009). Arctic deltas are likely more vulnerable than their temperate counterparts due to the presence of thermokarst lakes in permafrost, which are sensitive to rapid Arctic warming (Emmerton et al., 2007; Piliouras & Rowland, 2020; Walker, 1998). Pan-arctic thermokarst lake coverage is responding to warmer temperatures in complex ways, as temperature-driven ground ice loss drives lake growth via retrogressive thaw slumping along lake shorelines (Grosse et al., 2013) but also generates surface and sub-surface hydrologic connectivity that can cause lake drainage (Grosse et al., 2013; Jones et al., 2020; Rowland et al., 2011; Yoshikawa & Hinzman, 2003). Observed changes in lake area over the last 50 years have shown both positive and negative trends depending on local hydrology, climate, permafrost zonation, ice content, landscape age, and geomorphic setting (Arp et al., 2011; Chen et al., 2012; Jones et al., 2011; Nitze et al., 2018; Plug et al., 2008; Smith et al., 2005). Irrespective of whether lake coverage is expanding or decreasing, change is expected to have consequences for the permafrost carbon cycle, as thermokarst lake expansion accelerates permafrost thaw and expedites the release of previously frozen carbon into the atmosphere as methane and CO_2, while lake drainage may slow permafrost-thaw and associated carbon emissions (van Huissteden et al., 2011). Major arctic deltas store approximately 91 $\pm$ 39 Pg-Carbon, potentially making them significant sources of future carbon emissions (Schuur et al., 2015). Moreover, thermokarst lakes in deltas modulate transport of riverine freshwater, sediment, and nutrient fluxes to the Arctic ocean, by trapping and holding sediment (Marsh et al., 1999; Piliouras & Rowland, 2020) and modifying the residence times and pathways of nutrient transport through the delta (Lesack & Marsh, 2010; Squires et al., 2009; Tank et al., 2009). Therefore, changing deltaic lake coverage and its spatial

distribution will also alter the timing and magnitudes of riverine fluxes to the Arctic Ocean, which has broader implications for near-shore circulation and ecosystem productivity (Lique et al., 2016).

We hypothesize that lake size variability and spatial arrangement across arctic deltas (Figure 1) may encode information on climate influence in permafrost environments, akin to how channel network structure is a signature of the riverine, tidal, and fluvial fluxes which shape temperate deltas (Nienhuis et al., 2016, 2018; Tejedor et al., 2015b, 2015a, 2016, 2017). In particular, we hypothesize that two primary drivers of lake size variability across deltas are ice content and climate and test this hypothesis quantitatively. Physically we expect that colder deltas have thicker permafrost which is able to support larger lakes, by preventing connection to the sub-permafrost groundwater table that can lead to eventual lake drainage (Grosse et al., 2013; Walvoord & Kurylyk, 2016; Yoshikawa & Hinzman, 2003) or diminished lake growth rates. We also expect that deltas with greater soil ice fraction will have larger lakes as soil ice acts as a subsurface hydraulic barrier, while soil ice melt induces subsidence and therefore lake growth. Discovering and quantifying data-driven relationships between lake size and ice content or temperature will be useful for constraining physical models and predicting future arctic delta morphology in a warmer climate.

However, a challenge in assessing the climatic signature on thermokarst lake sizes is the significant interannual (Grosse et al., 2013; Rey et al., 2019) and seasonal variability (Chen et al., 2012, 2013; Cooley et al., 2019; Vulis et al., 2020) in lake area which makes it difficult to distinguish perennial waterbodies (lakes) from ephemerally inundated depressions (wetlands) using the short summertime window of available spaceborne observations. In particular, seasonal water may inundate ephemeral wetlands, which would be misidentified as perennially inundated lakes from remote sensing imagery. The processes underlying ephemeral wetland versus perennial

lake formation are distinct, as lakes are the result of thermokarst-driven growth and evolution (Grosse et al., 2013), while wetlands are the result of hydrologic variability, and as defined in this study only seasonally inundated (Le & Kumar, 2014). Mixing of the two waterbodies is certain to hide causative patterns and signatures, as lakes and wetlands have different time scales of thermal impact on the landscape, and are thus expected to show different expressions of their size distribution and their dependence on climate.

2. Study sites, data, and lake and wetland extraction

Lake and wetland size distributions on 12 arctic deltas characterized by a range of air temperature and ice content across Siberia (Indigirka, Kolyma, Lena, Nadym, Ob, Pur, Yana, and Yenisei), Canada (Mackenzie), and Alaska (Colville, Kobuk, and Yukon) were examined (Figure 1). The deltas include those formed by the six arctic rivers with the greatest discharge and other major rivers along the Siberian and Alaskan coastlines. Lakes and wetlands were extracted over the subaerial portion of each delta, which was delineated using Google Earth. Delta Mean Annual Air Temperature (MAAT) was obtained from 2000-2016 using the 15-km spatial resolution Arctic Systems Reanalysis V2 (Bromwich et al., 2017). Delta soil ice content was estimated from a 12.5-km spatial resolution ice classification map (Brown et al., 1997).

To distinguish between hydrologically perennial lakes and ephemeral wetlands, we utilized the spatiotemporal interannual variability of water coverage over each delta from 1999 to 2018. We used the Landsat-derived, 30-m spatial resolution Global Surface Water (GSW) dataset which provides monthly-composited water masks from March 1984 to December 2018 that classify the landscape into 30-m pixels that are land, water, or no data (i.e. unable to classify due to cloud cover, Landsat-7 striping, or snow and ice cover) (Pekel et al., 2016). Due to sparse data availability prior to 1999 on most deltas, we only analyzed the period from 1999 to 2018, and to

remove the effect of significant snowmelt and spring time flooding we only analyzed July water masks, similar to other studies (Muster et al., 2019; Nitze et al., 2018). We only examined the subaerial portion of each delta, manually delineated using Google Earth.

To identify and separate lakes from wetlands, we first computed for every pixel i the July "water pixel occurrence", w_i, as the fraction of Julys from 1999 to 2018 for which the pixel was classified as water, discarding no-data pixels (Figure 2a). The water pixel occurrence w_i can take values from 0 to 1, with $w_i = 1$ if and only if the pixel was classified as water for the whole record and $w_i = 0$ if and only if the pixel was classified as land for the whole record. Second, we identified a reference year, y^*, with water coverage on the subaerial delta closest to that of the temporal average over the 20-year period of record and sufficient data quality, i.e. greater than 99% pixels classified as land or water and no significant geo-referencing (collocation) errors, and used this year to identify individual waterbodies using 8-neighbor connected component analysis (see Supplementary Material, Figures S1 to S3 for details on selection of y^*). Third, we classified the waterbodies identified in year y^* into lakes and wetlands using the water pixel occurrence, w_i. For each waterbody, $O_k^{y^*}$, we computed the "occurrence index" B_k as the mean of w_i for all pixels i within $O_k^{y^*}$, which corresponds to the fraction of pixels within the waterbody that were on average occupied by water over the 20 years (Julys) of record. A waterbody was then classified as a lake if B_k exceeded a threshold value θ and as a wetland if B_k was less than θ. We evaluated the results over a range of θ values, from $\theta = 0.80$ to $\theta = 0.90$, to account for differences in the flooding regime across different deltas and to test the robustness of our results (Tables S1 to S3, Figures S4 and S5). The lake and wetland size distributions shown in Figures 3 and 4 are extracted at a threshold value of $\theta = 0.85$. Only waterbodies at least 5,400 m^2 (i.e. 6 pixels) in size were included in our analysis to reduce estimation errors at small areas. We tested the robustness of our

methodology by performing a duplication, wherein we selected an alternative reference year, y^*_{alt}, with similar water coverage and data quality to extract waterbody extents and repeated the analysis (Supplementary Material, Table S4, and Figures S4 and S5). All analyses were performed in R using geospatial and image processing packages (Gillespie, 2015; Hijmans, 2020; Pau et al., 2010; Pebesma, 2018, 2020).

3. Lake size distributions and a proportionate growth model

From a simple thermodynamical perspective, thermokarst lakes are thermal reservoirs, which interact with their surroundings via heat exchange. In particular, unfrozen lake waters are net heat sources, thawing the surrounding ice-rich soil which leads to lake basin expansion (Grosse et al., 2013). As larger lakes have a larger thermal inertia, they remain unfrozen for longer periods (Grosse et al., 2013) and maintain larger lake to soil temperature gradients, which enables them to grow at faster rates. Thus, based on this simple thermodynamical argument, and on field observations (Jones et al., 2011), we can postulate that thermokarst lake growth is compatible with a stochastic proportionate growth model (Crow & Shimizu, 1988; Mitzenmacher, 2004) (i.e. growth rate proportional to lake size), where stochasticity arises from the variability of soil properties which modulate growth. A key property of this general class of proportionate growth models is that they generate objects (in our case lakes) with sizes obeying a lognormal (LN) distribution (Supplementary Material) (Crow & Shimizu, 1988). Thus, our expectation based on simple physical arguments is that arctic deltas should universally exhibit lakes whose sizes are lognormally distributed. In particular, since we only observe lake sizes above 5,400 m^2 (6 pixels) we expect lake sizes to follow a truncated lognormal distribution (Equation 1):

$$f_x(x;\nu,\beta^2) = \begin{cases} 0 & for\ x < x_{min} \\ \frac{1}{x\beta\sqrt{2\pi}} e^{\frac{-(ln(x)-\nu)^2}{2\beta^2}} \Big/ \left[1-\Phi\left(\frac{ln(x_{min})-\nu}{\beta}\right)\right] & for\ x \geq x_{min} \end{cases}, \quad (1)$$

where $\Phi(\cdot)$ is the cumulative distribution function (CDF) of a standard normal variable, ν is the scale parameter, β the shape parameter, and x_{min} the minimum value at which the LN is observed, here 5,400 m^2 (Clauset et al., 2009). When x_{min} approaches zero, the denominator approaches unity and Equation (1) is simply the LN distribution.

Having separated lakes and wetlands based on the methodology outlined in section 2, we examined the empirical probability density function (PDF) of lake sizes (Figure 3a). As postulated, we found that the examined lake sizes can be accurately described by a truncated LN distribution for the whole range of lake sizes (spanning 3.5 orders of magnitude) in the 12 deltas under study (see Quantile-Quantile (Q-Q) plots in Figure 3b). The rigorous Lilliefors-corrected Kolmogorov-Smirnov (KS) test (Clauset et al., 2009), shows that for every delta, the fitted LN distribution could not be rejected at the 5% significance level within the range of thresholds θ utilized for the identification of lakes from the general waterbody population (Tables S1 to S3). For most deltas, the LN fit could not be rejected over the entire range, but in several deltas the test outcome depended on the threshold, due to the fact that the hydrogeomorphological specificities of the different deltas can lead to potential suboptimal lake/wetland separation for certain threshold values and ranges of waterbody sizes. Furthermore, the robustness of the revealed universality of the LN distribution of lake sizes was confirmed by successfully testing that lake sizes are LN distributed when alternative years were used as reference to extract waterbodies (Table S4, Figure S4). Previous empirical (suggesting different distributions for arctic waterbodies) (Muster et al., 2019) and theoretical (suggesting a proportionate growth model) (Victorov et al., 2019) studies have failed to demonstrate this universality because thermokarst lakes and wetlands were analyzed

178 together (Table S5 and Figure S6), and as we show in the next section wetlands do exhibit a
179 different distribution.

180 **4. Wetland size distributions and an inundated topography model**

181 Arctic delta wetlands are, by definition, ephemeral waterbodies emerging on the delta top due
182 to local ice/snow melt and riverine flooding. Therefore, wetland sizes are expected to be highly
183 dependent on the seasonal delta hydrology, which controls overall delta wetness (hydrologic
184 forcing), and delta topography; the topography in turn constitutes the spatial layout for inundation,
185 and controls both the emergence of disjoint wetlands and their sizes for a given forcing. The
186 prevalence of power-law distributions describing the sizes of waterbodies emerging from
187 landscape inundation has been extensively documented (Bertassello et al., 2018; Cael & Seekell,
188 2016; Le & Kumar, 2014; Mandelbrot, 1982). For instance, recent analysis of the sizes of
189 waterbodies identified from inundating low-relief topography and observed wetlands in the
190 contiguous United States were found to exhibit power law distribution of areas consistent with
191 inundated fractal topography (Bertassello et al., 2018; Le & Kumar, 2014). Therefore, our
192 hypothesis was that the Arctic delta wetlands will follow a similar distribution. The form of the
193 power law PDF used in this study is given in Equation (2), where x_0 is the minimum size above
194 which the power law is fit and α is the power law exponent (Clauset et al., 2009):

195 $$f_X(x;\alpha) = \frac{\alpha-1}{x_0}\left(\frac{x}{x_0}\right)^{-\alpha}, x > x_0 \quad (2)$$

196 We observed that wetland size distributions in the 12 arctic deltas indeed show strong evidence
197 of being power law distributed (log-log linearity over two orders of magnitude in Figure 3c). Using
198 the robust methodology of Clauset et al. (2009) for power law testing and fitting, we found that
199 the power-law hypothesis for wetland sizes could not be rejected at the 5% significance level with

a Lilliefors-corrected KS test for all 12 deltas (Tables S1 to S3). As with lakes, the power law distribution of wetland sizes is robust with respect to the threshold θ, which establishes the separation of waterbodies into lakes and wetlands (Tables S1 to S3). Moreover, the robustness of our hypothesis was verified by extracting waterbodies and identifying wetlands in an alternative reference year, wherein again most deltas displayed power law wetland size distributions (Table S4, Figure S4).

Recent literature has hypothesized that lakes in the Arctic are consistent with landscape inundation mechanisms (Muster et al., 2019). This hypothesis was grounded on the finding that empirical statistics of waterbodies obey two relationships (a linear relationship between conditional mean and conditional variance and a hyperbolic relationship between conditional mean and conditional skewness) which are consistent with those arising from an inundation model experiment (Muster et al., 2019). However, as we show here (Supplementary Material, Figure S8) these same relationships arise from a proportionate growth model and a LN distribution, cautioning their use for distinguishing between the power-law and LN probability distributions and making physical inferences.

5. Climate trends

How will the Arctic look like in a warmer future is a question of interest due to the critical impacts that changes in lake and wetland coverage will have on methane emissions (Engram et al., 2020; van Huissteden et al., 2011; Petrescu et al., 2010), release of old carbon (Grosse et al., 2013; Rowland et al., 2010), re-plumbing of surface-subsurface hydrologic partitioning (Walvoord & Kurylyk, 2016), and changes in water and biogeochemical cycling to the ocean (Piliouras et al., 2021; Piliouras & Rowland, 2020). Although physical models could be used to project such changes, their complexity and uncertainty in parameterizations makes it difficult to implement

them over large areal extents and long periods of time (van Huissteden et al., 2011; Kessler et al., 2012; Plug & West, 2009). We posit that if robust relationships between lake size distributions and climate variables can be established based on analysis of deltas across a gradient of temperature, soil ice content and permafrost coverage, valuable quantitative insight can be gained for the future. More specifically, we pose the hypothesis that lake sizes encode the signature of climate while ephemeral wetlands are mostly agnostic to it.

We have tested this hypothesis by analyzing the relationships between mean lake and wetland size (areal extent) with respect to MAAT and soil ice content. The data suggest that the mean thermokarst lake size increases by $9 \cdot 10^4$ m^2, i.e. doubling, over a 12°C decrease in the average 2000 to 2016 MAAT (Bromwich et al., 2017), indicating that colder deltas have significantly larger lakes on average (Figure 4a). Modern MAAT may not be representative of paleoclimatic temperature variability; however mean lake size also has a significant linear relationship (p = 0.028, R^2 = 0.40) with delta apex latitude, which is a reasonable proxy for historical temperature differences between the deltas, strongly supporting a temperature to lake size relationship. Mean lake size also generally positively relates to soil ice content, as higher ice content on the delta may support lake growth due to greater settlement from ice melt (Grosse et al., 2013), with lower ice content associated with smaller lakes (Figure 4a). A similar trend between lake sizes and MAAT is observed when an alternative reference year is used to extract waterbodies in (Figure S5a), supporting the robustness of this dependence. On the other hand, the data show no relationship between mean wetland size and MAAT (Figures 4b, Figure S5b). Also expected, but confirmed, mixing the two waterbodies makes it hard to detect the climatic signal on the landscape. Indeed, a joint analysis reveals a non-significant relationship with MAAT (Figure S6d).

The observed relationship for mean lake size and MAAT is attributed to the greater capacity of colder deltas to support large lakes due to their presumably thicker and cooler permafrost, which prevents sub-lake taliks from connecting to the sub-permafrost groundwater table (Walvoord & Kurylyk, 2016). This connection in low relief deltaic environments would reduce lake level as river stage recedes through the summer, transitioning the margins of perennially inundated lakes to ephemerally inundated, thereby reducing lateral thermal fluxes from the lake to the surrounding permafrost, i.e. diminishing lake growth and decreasing the observed size of perennially inundated lakes (Figures 4c and 4d). Such an effect would be clearest in large lakes which have deep taliks (Grosse et al., 2013), and indeed, we found that the peripheries of large lakes were inundated more often on average over the period of record on warmer deltas compared with colder deltas (Figure 4e). Note that the fraction of the periphery that remains water (inundated) on average over the period of record (Figure 4e) is computed as the average w_i of all pixels bordering the lake (in an 8-neighbor sense), and then the average of large lakes (defined as those with areas between 10^5 and 10^6 m^2) over the entire delta computed to obtain a representative value.

Such a relationship may also occur due to evapotranspiration rates being higher on warmer deltas, which lead to greater lake margin loss. However, we found that average June-July precipitation minus evapotranspiration (P-ET, i.e. the vertical hydrologic budget) (Bromwich et al., 2017) over the delta is uncorrelated with MAAT, and therefore P-ET does not explain the relationship between delta temperature and how often lake peripheries are inundated (Figure S5d). This mechanism could be validated in future studies by imaging subsurface permafrost structure across the deltas which has been done in other permafrost environments (Rey et al., 2019).

6. Perspectives and Conclusions

By harnessing more than 20 years of remote sensing data over the Arctic, we have developed a methodology to classify waterbodies, depending on their year-to-year variability, as lakes (perennial) and wetlands (ephemeral). The statistical distributions of lake and wetland sizes are distinct and appear to be universal across arctic deltas, reflecting the respective underlying mechanisms driving the formation and evolution of those waterbodies. Specifically, it was found that thermokarst lake sizes obey a lognormal distribution, which can be interpreted as the emergent signature of the thermal mechanism driving lake formation and growth. On the other hand, wetland sizes were found to exhibit a power law distribution compatible with landscape inundation models relevant to ephemeral waterbodies (Bertassello et al., 2018; Le & Kumar, 2014). The difference between the underlying forming mechanisms leads also to different expectations with respect to possible relationships with climatic variables. Indeed, our results reveal a significant trend between mean lake size and mean annual air temperature, supporting the hypothesis that colder environments are able to grow and sustain larger thermokarst lakes, while no signature of climate is found in the mean wetland sizes. The power law exponents of the wetland size distributions were found to range between 1.8 and 2.8 (a smaller exponent indicates a thicker tail of the PDF) and further analysis of high-resolution topography is expected to provide additional insight on this range. The decreasing trend of mean lake size with warmer temperatures found here can form the basis for future lake area change projections, recognizing however that the relationship from the 12 examined deltas, although statistically significant, explains only 40% of the variance and lake change may display significant spatial variability (Chen et al., 2012). Spatially resolved permafrost depth and ground ice content on the deltas (Rey et al., 2019), as well as analysis of physically-based models forced with different climate scenarios (Coon et al., 2019; Overeem et al., 2018) is

291 needed to better understand cause-and-effect and derive relationships that can serve as the basis of
292 projections of landscape change (e.g. increased water ephemerality under warming scenarios) and
293 associated carbon cycle impacts in specific delta environments.

294 **Acknowledgements**

295 L.V. was supported under the NASA Earth and Space Science Fellowship Program Grant
296 80NSSC18K1409 and the UC-National Lab In-Residence Graduate Fellowship Grant
297 L21GF3569. E.F-G., A.T., and L.V. received support from NSF Earth Sciences Directorate Grant
298 EAR-1811909 and the UK Research and Innovation Global Challenges Research Fund Living
299 Deltas Hub Grant NES0089261. I.Z. received support from NSF Earth Sciences Directorate Grant
300 EAR-1723033. J.C.R. received support as part of the Interdisciplinary Research for Arctic Coastal
301 Environments (InteRFACE) project through the Department of Energy, Office of Science,
302 Biological and Environmental Research (BER) Regional and Global Model Analysis (RGMA)
303 program. We thank the Luca de Felice from the Global Surface Water team for his assistance in
304 addressing geo-referencing and pyramiding issues in the monthly water masks.

305 **Data Availability**

306 The Global Surface Water monthly water masks are available via Google Earth Engine
307 (https://earthengine.google.com/). The Arctic Systems Reanalysis V2 data is available from
308 University Corporation for Atmospheric Research (UCAR) Research Data Archive (RDA)
309 (https://rda.ucar.edu/datasets/ds631.1/). The ice content data is available from the National Snow
310 and Ice Data Center (NSIDC) (https://nsidc.org/data/ggd318). Code to reproduce this analysis are
311 available from the corresponding author upon request.

312

References

Arp, C. D., Jones, B. M., Urban, F. E., & Grosse, G. (2011). Hydrogeomorphic processes of thermokarst lakes with grounded-ice and floating-ice regimes on the Arctic coastal plain, Alaska. *Hydrological Processes*, *25*(15), 2422–2438. https://doi.org/10.1002/hyp.8019

Bertassello, L. E., Rao, P. S. C., Jawitz, J. W., Botter, G., Le, P. V. V., Kumar, P., & Aubeneau, A. F. (2018). Wetlandscape Fractal Topography. *Geophysical Research Letters*, *45*(14), 6983–6991. https://doi.org/10.1029/2018GL079094

Bromwich, D. H., Wilson, A. B., Bai, L., Liu, Z., Barlage, M., Shih, C.-F., et al. (2017). The Arctic System Reanalysis Version 2. *Bulletin of the American Meteorological Society*, (April), BAMS-D-16-0215.1. https://doi.org/10.1175/BAMS-D-16-0215.1

Brown, J., Ferrians, O. J., Heginbottom, J. A., & Melnikov, E. S. (1997). *Circum-Arctic map of permafrost and ground-ice conditions*. Washington DC. Retrieved from https://nsidc.org/data/ggd318

Cael, B. B., & Seekell, D. A. (2016). The size-distribution of Earth's lakes. *Scientific Reports*, *6*(1), 29633. https://doi.org/10.1038/srep29633

Chen, M., Rowland, J. C., Wilson, C. J., Altmann, G. L., & Brumby, S. P. (2012). Temporal and spatial pattern of thermokarst lake area changes at Yukon Flats, Alaska. *Hydrological Processes*, *28*(3), 837–852. https://doi.org/10.1002/hyp.9642

Chen, M., Rowland, J. C., Wilson, C. J., Altmann, G. L., & Brumby, S. P. (2013). The importance of natural variability in lake areas on the detection of permafrost degradation: A case study in the Yukon Flats, Alaska. *Permafrost and Periglacial Processes*, *24*(3), 224–240. https://doi.org/10.1002/ppp.1783

Clauset, A., Shalizi, C. R., & Newman, M. E. J. (2009). Power-Law Distributions in Empirical Data. *SIAM Review*, *51*(4), 661–703. https://doi.org/10.1137/070710111

Cooley, S. W., Smith, L. C., Ryan, J. C., Pitcher, L. H., & Pavelsky, T. M. (2019). Arctic-Boreal lake dynamics revealed using CubeSat imagery. *Geophysical Research Letters*, *46*, 2018GL081584. https://doi.org/10.1029/2018GL081584

Coon, E., Svyatsky, D., Jan, A., Kikinzon, E., Berndt, M., Atchley, A., et al. (2019, September). Advanced Terrestrial Simulator. https://doi.org/10.11578/dc.20190911.1

Crow, E. L., & Shimizu, K. (1988). *Lognormal Distributions Theory and Applications* (1st Editio). New York: Marcel Dekker.

Emmerton, C. A., Lesack, L. F. W., & Marsh, P. (2007). Lake abundance, potential water storage, and habitat distribution in the Mackenzie River Delta, western Canadian Arctic. *Water Resources Research*, *43*(5), 1–14. https://doi.org/10.1029/2006WR005139

Engram, M., Walter Anthony, K. M., Sachs, T., Kohnert, K., Serafimovich, A., Grosse, G., & Meyer, F. J. (2020). Remote sensing northern lake methane ebullition. *Nature Climate Change*, *10*(6), 511–517. https://doi.org/10.1038/s41558-020-0762-8

Gillespie, C. S. (2015). Fitting Heavy Tailed Distributions: The poweRlaw Package. *Journal of*

Statistical Software, *64*(2). https://doi.org/10.18637/jss.v064.i02

Grosse, G., Jones, B., & Arp, C. (2013). *Thermokarst Lakes, Drainage, and Drained Basins*. *Treatise on Geomorphology* (Vol. 8). Elsevier Ltd. https://doi.org/10.1016/B978-0-12-374739-6.00216-5

Hijmans, R. J. (2020). raster: Geographic Data Analysis and Modeling. Retrieved from https://cran.r-project.org/package=raster

van Huissteden, J., Berrittella, C., Parmentier, F. J. W., Mi, Y., Maximov, T. C., & Dolman, A. J. (2011). Methane emissions from permafrost thaw lakes limited by lake drainage. *Nature Climate Change*, *1*(2), 119–123. https://doi.org/10.1038/nclimate1101

Jones, B. M., Grosse, G., Arp, C. D., Jones, M. C., Walter Anthony, K. M., & Romanovsky, V. E. (2011). Modern thermokarst lake dynamics in the continuous permafrost zone, northern Seward Peninsula, Alaska. *Journal of Geophysical Research*, *116*(3), G00M03. https://doi.org/10.1029/2011JG001666

Jones, B. M., Arp, C. D., Grosse, G., Nitze, I., Lara, M. J., Whitman, M. S., et al. (2020). Identifying historical and future potential lake drainage events on the western Arctic coastal plain of Alaska. *Permafrost and Periglacial Processes*, *31*(1), 110–127. https://doi.org/10.1002/ppp.2038

Kessler, M. A., Plug, L. J., & Walter Anthony, K. M. (2012). Simulating the decadal- to millennial-scale dynamics of morphology and sequestered carbon mobilization of two thermokarst lakes in NW Alaska. *Journal of Geophysical Research: Biogeosciences*, *117*(1), 1–22. https://doi.org/10.1029/2011JG001796

Le, P. V. V, & Kumar, P. (2014). Power law scaling of topographic depressions and their hydrologic connectivity. *Geophysical Research Letters*, *41*(5), 1553–1559. https://doi.org/10.1002/2013GL059114

Lesack, L. F. W., & Marsh, P. (2010). River-to-lake connectivities, water renewal, and aquatic habitat diversity in the Mackenzie River Delta. *Water Resources Research*, *46*(12), 1–16. https://doi.org/10.1029/2010WR009607

Lique, C., Holland, M. M., Dibike, Y. B., Lawrence, D. M., & Screen, J. A. (2016). Modeling the Arctic freshwater system and its integration in the global system: Lessons learned and future challenges. *Journal of Geophysical Research: Biogeosciences*, *121*(3), 540–566. https://doi.org/10.1002/2015JG003120

Mandelbrot, B. B. (1982). *The Fractal Geometry of Nature* (1st ed.). New York.

Marsh, P., Lesack, L. F. W., & Roberts, A. (1999). Lake sedimentation in the Mackenzie Delta, NWT. *Hydrological Processes*, *13*(16), 2519–2536. https://doi.org/10.1002/(SICI)1099-1085(199911)13:16<2519::AID-HYP935>3.0.CO;2-T

Mitzenmacher, M. (2004). A Brief History of Generative Models for Power Law and Lognormal Distributions. *Internet Mathematics*, *1*(2), 226–251. https://doi.org/10.1080/15427951.2004.10129088

Muster, S., Riley, W. J., Roth, K., Langer, M., Cresto Aleina, F., Koven, C. D., et al. (2019). Size

Distributions of Arctic Waterbodies Reveal Consistent Relations in Their Statistical Moments in Space and Time. *Frontiers in Earth Science*, *7*(January), 1–15. https://doi.org/10.3389/feart.2019.00005

Nienhuis, J. H., Ashton, A. D., & Giosan, L. (2016). Littoral steering of deltaic channels. *Earth and Planetary Science Letters*, *453*(April 2018), 204–214. https://doi.org/10.1016/j.epsl.2016.08.018

Nienhuis, J. H., Hoitink, A. J. F. T., & Törnqvist, T. E. (2018). Future Change to Tide-Influenced Deltas. *Geophysical Research Letters*, *45*(8), 3499–3507. https://doi.org/10.1029/2018GL077638

Nienhuis, J. H., Ashton, A. D., Edmonds, D. A., Hoitink, A. J. F., Kettner, A. J., Rowland, J. C., & Törnqvist, T. E. (2020). Global-scale human impact on delta morphology has led to net land area gain. *Nature*, *577*(7791), 514–518. https://doi.org/10.1038/s41586-019-1905-9

Nitze, I., Grosse, G., Jones, B. M., Romanovsky, V. E., & Boike, J. (2018). Remote sensing quantifies widespread abundance of permafrost region disturbances across the Arctic and Subarctic. *Nature Communications*, *9*(1), 5423. https://doi.org/10.1038/s41467-018-07663-3

Obu, J., Westermann, S., Bartsch, A., Berdnikov, N., Christiansen, H. H., Dashtseren, A., et al. (2019). Northern Hemisphere permafrost map based on TTOP modelling for 2000–2016 at 1 km2 scale. *Earth-Science Reviews*, *193*(October 2018), 299–316. https://doi.org/10.1016/j.earscirev.2019.04.023

Overeem, I., Jafarov, E., Wang, K., Schaefer, K., Stewart, S., Clow, G., et al. (2018). A Modeling Toolbox for Permafrost Landscapes. *Eos*, *99*. https://doi.org/10.1029/2018EO105155

Pau, G., Fuchs, F., Sklyar, O., Boutros, M., & Huber, W. (2010). EBImage-an R package for image processing with applications to cellular phenotypes. *Bioinformatics*, *26*(7), 979–981. https://doi.org/10.1093/bioinformatics/btq046

Pebesma, E. (2018). Simple Features for R: Standardized Support for Spatial Vector Data. *The R Journal*, *10*(1), 439. https://doi.org/10.32614/RJ-2018-009

Pebesma, E. (2020). stars: Spatiotemporal Arrays, Raster and Vector Data Cubes. Retrieved from https://cran.r-project.org/package=stars

Pekel, J.-F., Cottam, A., Gorelick, N., & Belward, A. S. (2016). High-resolution mapping of global surface water and its long-term changes. *Nature*, *540*(7633), 418–422. https://doi.org/10.1038/nature20584

Petrescu, A. M. R., Van Beek, L. P. H., Van Huissteden, J., Prigent, C., Sachs, T., Corradi, C. A. R., et al. (2010). Modeling regional to global CH4 emissions of boreal and arctic wetlands. *Global Biogeochemical Cycles*, *24*(4), 1–12. https://doi.org/10.1029/2009GB003610

Piliouras, A., & Rowland, J. C. (2020). Arctic River Delta Morphologic Variability and Implications for Riverine Fluxes to the Coast. *Journal of Geophysical Research: Earth Surface*, *125*(1), 1–20. https://doi.org/10.1029/2019JF005250

Piliouras, A., Lauzon, R., & Rowland, J. C. (2021). Unraveling the Combined Effects of Ice and Permafrost on Arctic Delta Morphodynamics. *Journal of Geophysical Research: Earth Surface*, *126*(4), 1–17. https://doi.org/10.1029/2020JF005706

Plug, L. J., & West, J. J. (2009). Thaw lake expansion in a two-dimensional coupled model of heat transfer, thaw subsidence, and mass movement. *Journal of Geophysical Research*, *114*(F1), F01002. https://doi.org/10.1029/2006JF000740

Plug, L. J., Walls, C., & Scott, B. M. (2008). Tundra lake changes from 1978 to 2001 on the Tuktoyaktuk Peninsula, western Canadian Arctic. *Geophysical Research Letters*, *35*(3), L03502. https://doi.org/10.1029/2007GL032303

Rey, D. M., Walvoord, M., Minsley, B., Rover, J., & Singha, K. (2019). Investigating lake-area dynamics across a permafrost-thaw spectrum using airborne electromagnetic surveys and remote sensing time-series data in Yukon Flats, Alaska. *Environmental Research Letters*, *14*(2), 025001. https://doi.org/10.1088/1748-9326/aaf06f

Rowland, J. C., Jones, C. E., Altmann, G., Bryan, R., Crosby, B. T., Geernaert, G. L., et al. (2010). Arctic landscapes in transition: Responses to thawing permafrost. *Eos*, *91*(26), 229–230. https://doi.org/10.1029/2010EO260001

Rowland, J. C., Travis, B. J., & Wilson, C. J. (2011). The role of advective heat transport in talik development beneath lakes and ponds in discontinuous permafrost. *Geophysical Research Letters*, *38*(17), 1–5. https://doi.org/10.1029/2011GL048497

Schuur, E. A. G., McGuire, A. D., Schädel, C., Grosse, G., Harden, J. W., Hayes, D. J., et al. (2015). Climate change and the permafrost carbon feedback. *Nature*, *520*(7546), 171–179. https://doi.org/10.1038/nature14338

Smith, L. C., Sheng, Y., MacDonald, G. M., & Hinzman, L. D. (2005). Disappearing Arctic Lakes. *Science*, *308*(5727), 1429–1429. https://doi.org/10.1126/science.1108142

Squires, M. M., Lesack, L. F. W., Hecky, R. E., Guildford, S. J., Ramlal, P., & Higgins, S. N. (2009). Primary production and carbon dioxide metabolic balance of a lake-rich arctic river floodplain: Partitioning of phytoplankton, epipelon, macrophyte, and epiphyton production among lakes on the mackenzie delta. *Ecosystems*, *12*(5), 853–872. https://doi.org/10.1007/s10021-009-9263-3

Syvitski, J. P. M., Kettner, A. J., Overeem, I., Hutton, E. W. H., Hannon, M. T., Brakenridge, G. R., et al. (2009). Sinking deltas due to human activities. *Nature Geoscience*, *2*(10), 681–686. https://doi.org/10.1038/ngeo629

Tank, S. E., Lesack, L. F. W., & Hesslein, R. H. (2009). Northern Delta lakes as summertime CO2 absorbers within the arctic landscape. *Ecosystems*, *12*(1), 144–157. https://doi.org/10.1007/s10021-008-9213-5

Tejedor, A., Longjas, A., Zaliapin, I., & Foufoula-Georgiou, E. (2015a). Delta channel networks: 1. A graph-theoretic approach for studying connectivity and steady state transport on deltaic surfaces. *Water Resources Research*, *51*(6), 3998–4018. https://doi.org/10.1002/2014WR016577

Tejedor, A., Longjas, A., Zaliapin, I., & Foufoula-Georgiou, E. (2015b). Delta channel networks:

2. Metrics of topologic and dynamic complexity for delta comparison, physical inference, and vulnerability assessment. *Water Resources Research*, *51*(6), 4019–4045. https://doi.org/10.1002/2014WR016604

Tejedor, A., Longjas, A., Caldwell, R., Edmonds, D. A., Zaliapin, I., & Foufoula-Georgiou, E. (2016). Quantifying the signature of sediment composition on the topologic and dynamic complexity of river delta channel networks and inferences toward delta classification. *Geophysical Research Letters*, *43*(7), 3280–3287. https://doi.org/10.1002/2016GL068210

Tejedor, A., Longjas, A., Edmonds, D. A., Zaliapin, I., Georgiou, T. T., Rinaldo, A., & Foufoula-Georgiou, E. (2017). Entropy and optimality in river deltas. *Proceedings of the National Academy of Sciences*, *114*(44), 11651–11656. https://doi.org/10.1073/pnas.1708404114

Victorov, A. S., Orlov, T. V., Kapralova, V. N., Trapeznikova, O. N., Sadkov, S. A., & Zverev, A. V. (2019). Stochastic Modeling of Natural Lacustrine Thermokarst Under Stable and Unstable Climate. In *Natural Hazards and Risk Research in Russia* (pp. 241–267). https://doi.org/10.1007/978-3-319-91833-4_18

Vulis, L., Tejedor, A., Schwenk, J., Piliouras, A., Rowland, J., & Foufoula-Georgiou, E. (2020). Channel Network Control on Seasonal Lake Area Dynamics in Arctic Deltas. *Geophysical Research Letters*, *47*(7). https://doi.org/10.1029/2019GL086710

Walker, H. J. (1998). Arctic Deltas. *Journal of Coastal Research*, *14*(3), 719–738. Retrieved from http://www.jstor.org/stable/4298831

Walvoord, M. A., & Kurylyk, B. L. (2016). Hydrologic Impacts of Thawing Permafrost-A Review. *Vadose Zone Journal*, *15*(6), 1–20. https://doi.org/10.2136/vzj2016.01.0010

Yoshikawa, K., & Hinzman, L. D. (2003). Shrinking thermokarst ponds and groundwater dynamics in discontinuous permafrost near Council, Alaska. *Permafrost and Periglacial Processes*, *14*(2), 151–160. https://doi.org/10.1002/ppp.451

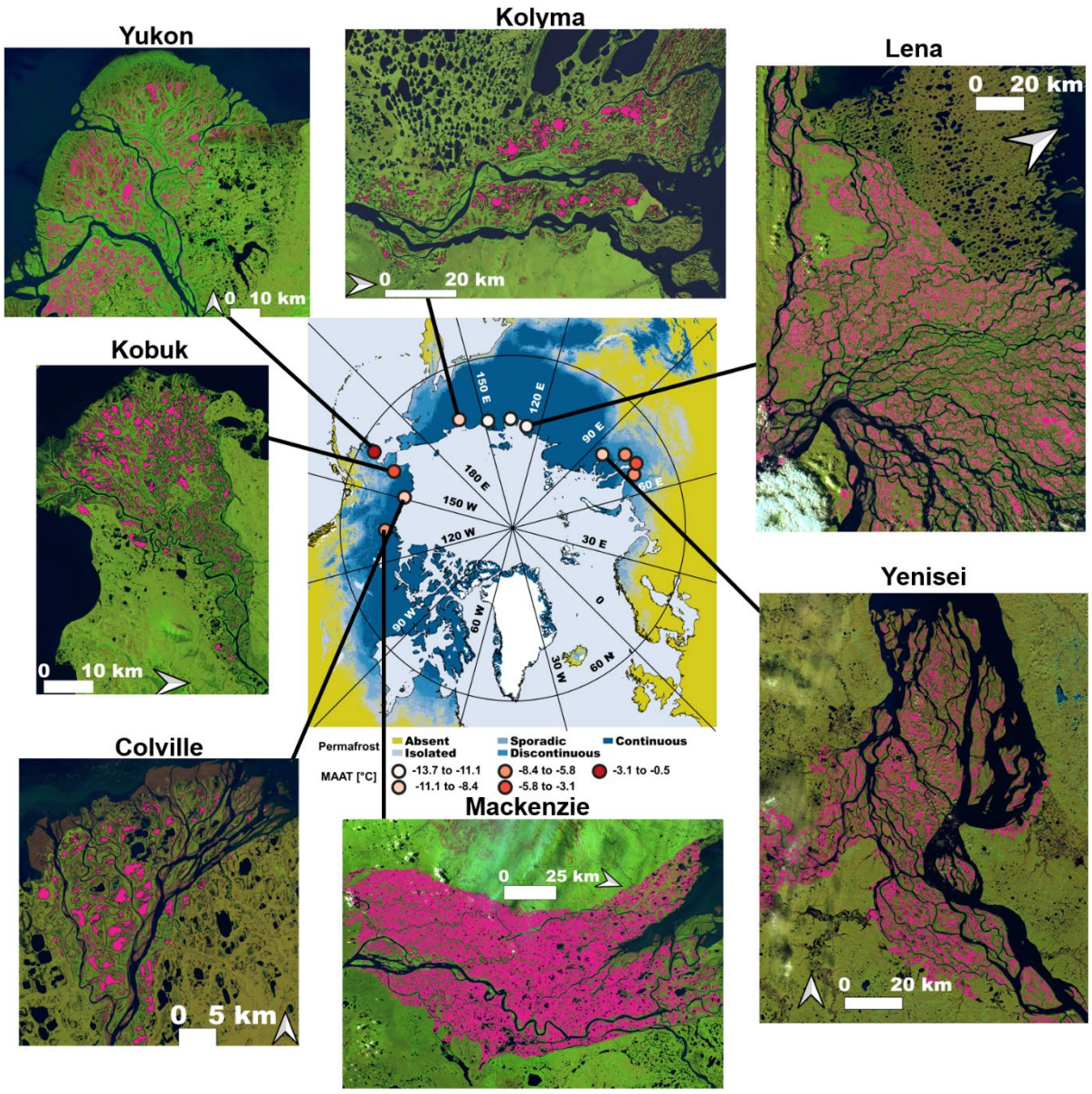

Figure 1. Arctic deltas examined in this study. Twelve arctic deltas (see colored open circles in the central panel for location) were examined along a range of Mean Annual Air Temperature (MAAT) and ice content. The central map shows delta locations, colored by 2000-2016 mean MAAT, estimated from the Arctic Systems Reanalysis V2 (Bromwich et al., 2017), and underlain by Arctic permafrost zonation (Obu et al., 2019). Summertime Landsat-8 scenes of 7 out of the 12 delta are shown with waterbodies identified from a single July Global Surface Water mask (Pekel et al., 2016) colored in pink.

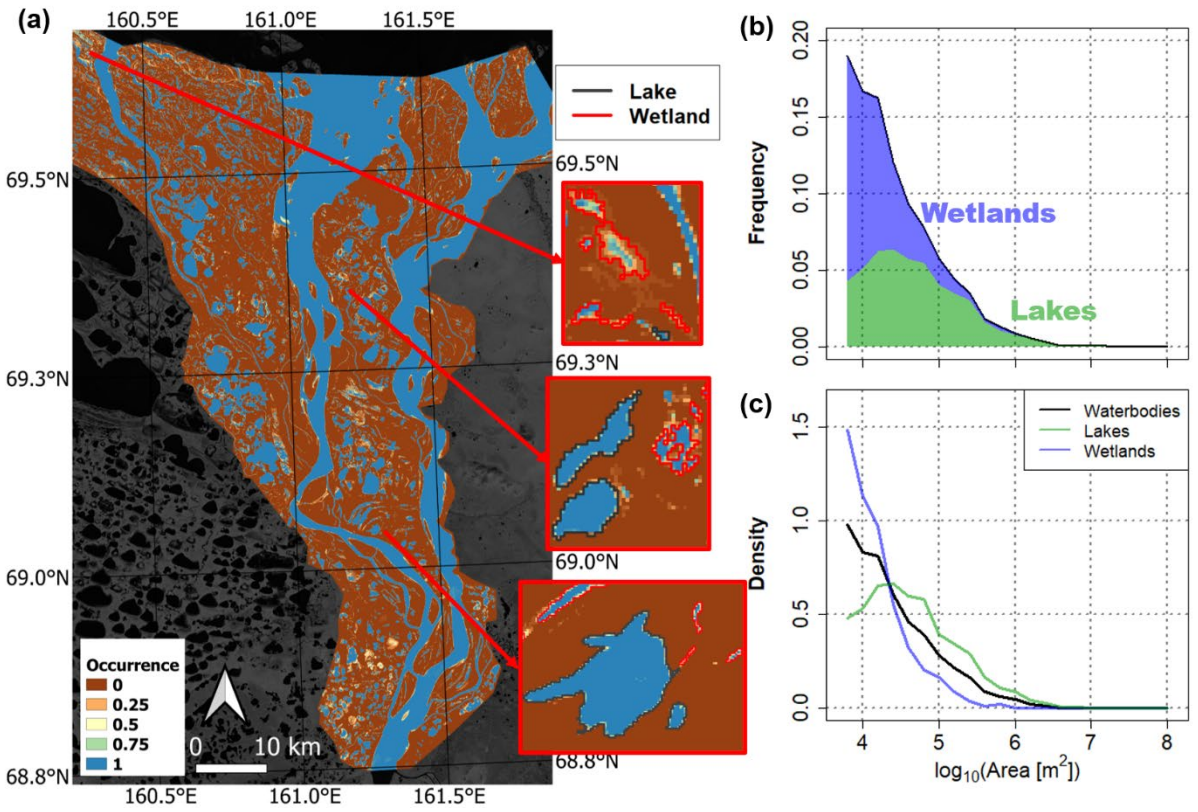

Figure 2. Example of waterbody classification procedure on Kolyma Delta. The waterbody classification procedure which marks waterbodies as either perennial lakes or ephemeral wetlands based on their July occurrence index, and the resulting size distribution. (a) July pixel water occurrence w_i over the Kolyma delta from 1999 to 2018. Brown indicates land pixels ($w_i = 0$) and blue indicates perennially inundated water pixels ($w_i = 1$), with colors in between indicating water pixels indicated only a fraction of the time. (b) The histogram of waterbody sizes is partitioned into the relative fraction of lakes (green) and wetlands (blue) at an occurrence index threshold $\theta = 0.85$. (c) The probability density function (PDF) of lake sizes in green and wetland sizes in blue, compared with waterbody sizes in black.

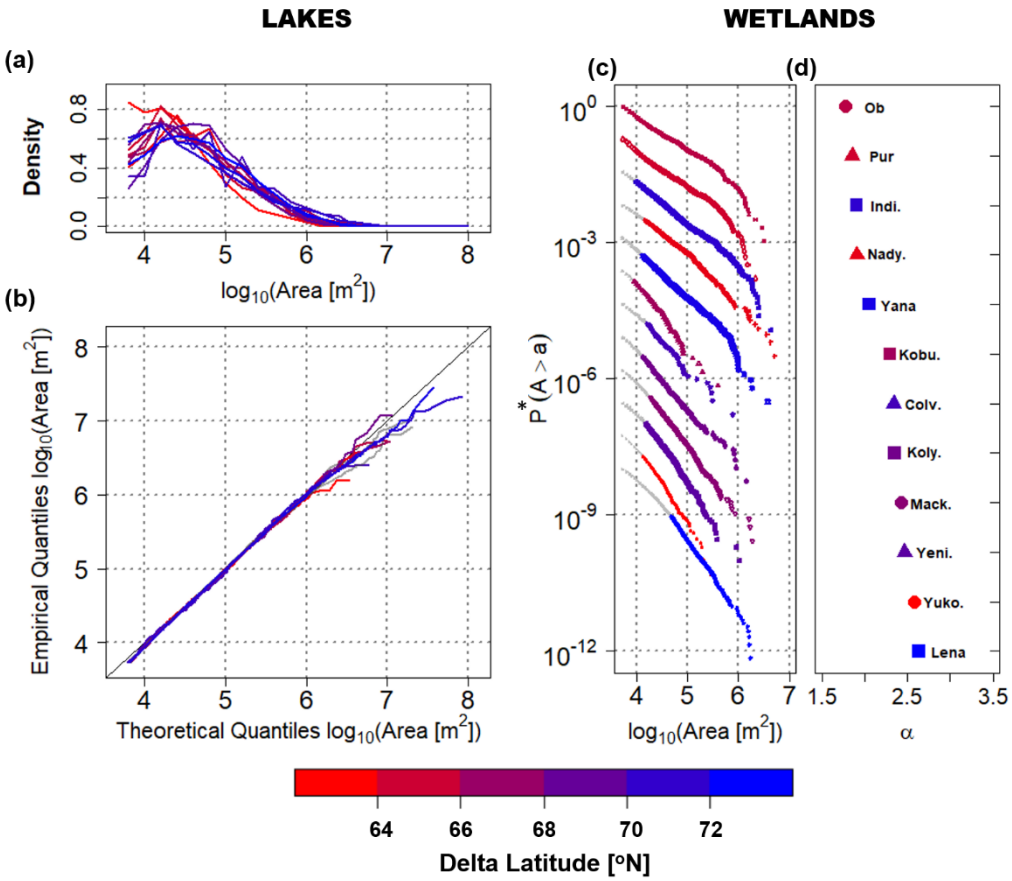

Figure 3. Size distributions of lakes and wetlands extracted at occurrence index threshold $\theta = 0.85$. (a) Lake size PDFs for the 12 deltas, (b) quantile-quantile plots of the lognormal with truncation from below at the minimum lake size (5,400 m^2) fitted to the lake size distribution. In (b) fitted distributions whose fit to data is rejected at the 5% significance level (KS test) are in grey. (c) Wetland size exceedance probability, (d) fitted power law exponent, α, of all 12 deltas. The exceedance probabilities in (c) are rescaled by a factor τ, i.e. $P^* = P\tau$, for visual display, and are ordered by increasing values of α to highlight the range of observed α. For each delta, power laws are fit to the colored points above the minimum wetland size, x_0, which was optimally determined using the procedure of Clauset et al. (2009). The power law parameter α in (d) is the scaling exponent of the PDF.

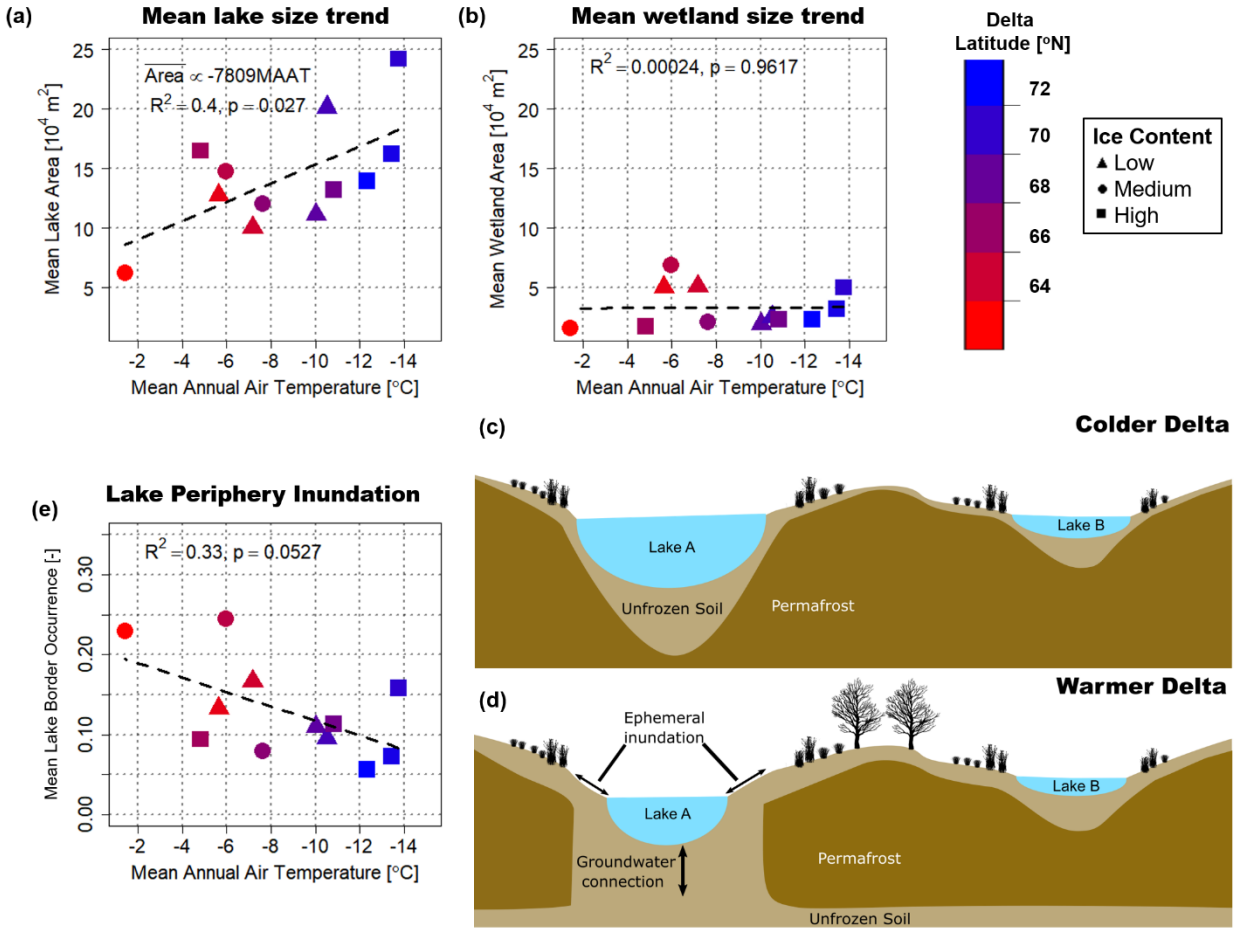

Figure 4. Lake and wetland size climate trends. (a) Scatterplot between mean lake size and MAAT showing a significant relationship between the two. (b) Scatterplot between mean wetland size and MAAT showing lack of a significant relationship. (c, d) The relationship between lake size and MAAT is attributed to colder deltas having thicker permafrost which prevents lakes from connecting to the sub-permafrost aquifer. In warmer deltas, connection to the sub-permafrost aquifer leads to greater lake level change over the summer, driving increased variability in inundation along the peripheries of lakes, and diminishing rates of thermally-driven lateral expansion. (e) Scatterplot between the fraction of the periphery of large lakes that remains water on average over the period of record and MAAT shows a weak (i.e. p~0.05) linear relationship, supporting this mechanism.

Climate signatures on lake and wetland size distributions in arctic deltas

Supplementary Material

Lawrence Vulis[1], Alejandro Tejedor[2,1], Ilya Zaliapin[3], Joel Rowland[4], and

Efi Foufoula-Georgiou[1,5]

[1]Department of Civil and Environmental Engineering, University of California Irvine, lvulis@uci.edu
[2]Department of Science and Engineering, Sorbonne University Abu Dhabi
[3]Department of Mathematics and Statistics, University of Nevada Reno
[4]Earth and Environmental Sciences Division, Los Alamos National Laboratory
[5]Department of Earth System Science, University of California Irvine

Table of Contents

I. Quality control of the Global Surface Water dataset

Thorough quality control of the water masks is necessary to reduce uncertainty in the estimated pixel water occurrence w_i and therefore the waterbody classification scheme. In particular, misclassified or poorly classified masks, e.g. where land pixels are classified as water or vice-versa, particularly in the presence of abundant unresolved pixels (i.e. pixels unable to be classified as land or water due to cloud cover, Landsat 7 striping, or other issues), introduce errors into the estimate of w_i, which lead to waterbody misclassification. To address this, we performed the following quality control procedure composed of a combination of quantitative rules and visual inspection on the GSW monthly water masks for all 12 deltas. First, for every delta we discarded from the analysis any mask over the period of record that had less than 10% of the study region resolved, as we observed misclassification errors for such poor-quality data. Second, we performed a visual inspection for significant misclassification errors, e.g. stripes of pixels classified as land or water or large swaths of the region appearing to be land only for a single year, and found only July 2016 on the Lena delta had to be discarded. Third, we identified and estimated mis-collocation errors in the GSW dataset of at least 1 pixel (30 meters) over the Yana delta from 2016 to 2018 and Lena delta from 2017 to 2018 relative to the masks from 1999 to 2015. These years were discarded from the computation of the July water pixel occurrence, w_i, but were used to estimate the average water cover since mis-collocation does not imply features were misclassified, only that their locations were shifted. No miscollocation on the order of one pixel (30-m) was observed on the other 10 deltas from 1999 to 2018. Note that the Pechora delta has not been considered in this work because of a large collocation error even in GSW v1.0 (i.e. years prior to 2016).

An example of the collocation errors is shown for the Yana delta, where waterbodies extracted from July 2018 are shifted to the north-west compared to waterbodies extracted from July 2011 (Figure S1). Due to interannual variability in surface water extent and a lack of ground control points, we were not able to compute the exact collocation error over the region and to correct the masks. Therefore, to estimate the magnitude of the miscollocation, we looked at the distribution of differences in waterbody centroids between different years, $(\Delta C_x, \Delta C_y)$. We found that the median of $(\Delta C_x, \Delta C_y) = (C_{x,2011} - C_{x,2018}, C_{y,2011} - C_{y,2018})$ was (29.24, -11.06) m, i.e. the median centroid difference between the two masks was approximately one pixel in the horizontal direction and a third of a pixel in the vertical. By examining the whole distribution of differences in waterbody centroids, we quantified that over 88% percent of waterbodies in 2018 were shifted to the southwest relative to the position of the same waterbodies in 2011 (i.e. over 88% of the centroids lay within the lower right quadrant of Figure S1b).

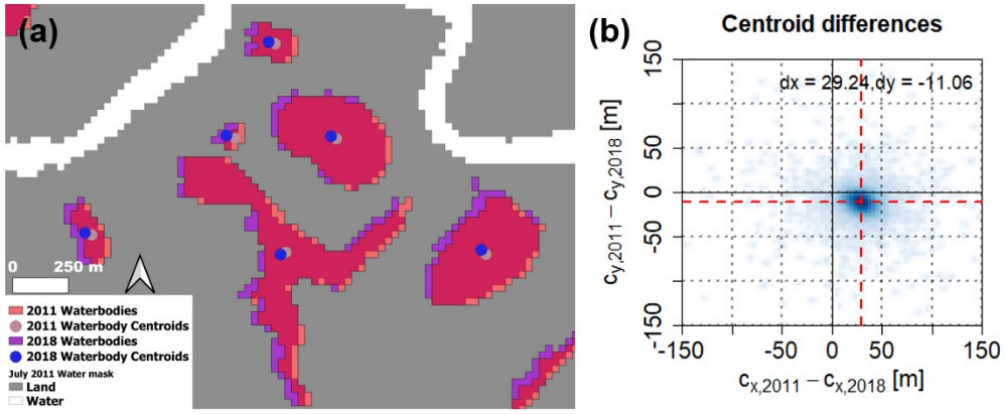

Figure S1. Collocation errors in the GSW dataset on the Yana delta. (a) Waterbodies from 2011 (red) and 2018 (purple) overlaid over the July 2011 water mask, with a clear offset between the two. The corresponding waterbody centroids are shown in brown and blue, respectively. (b) The distribution of centroid differences is shown with the median difference in each direction given by the red dashed line.

II. Hydrology of the deltas and choice of the year for waterbody mask extraction

To choose the reference year y^* in which to extract waterbody extents as objects and classify perennial lakes and ephemeral wetlands based on their year-to-year variability, we first computed for each delta and year the water cover, i.e. the fraction of valid (i.e. resolved as water or land) pixels that are classified as water over the subaerial delta, defining time series of July water cover from 1999 to 2018 (Figures S2 and S3). Then, we computed for each delta the average water cover over the period of record using the total number of valid pixels in each year as weights. Finally, y^* was chosen as the year with water cover closest to the average and at least 99% valid pixels. To test the robustness of the results, an alternative reference year, y^*_{alt} was also selected for each delta with a similar water cover to y^* and high data quality and the analysis repeated (S4 and Figures S4 and S5). To account for the heterogeneity in data quality across the range of analyzed systems, exceptions to these criteria had to be made for the Yukon, Lena, and Indigirka deltas. On the Yukon delta, the only two years satisfying the 99% valid pixel criterion were the 2008 and 2014, but these two are the wettest years on record, not years with typical hydrology. Therefore, 2017 and 2016 which had 98.7% and 98.9% valid pixels (slightly less than the 99% criterion), but close to average water cover were chosen as y^* and y^*_{alt}, respectively (Figure S2). On the Lena and Indigirka deltas only 2013 and 2016, respectively, had at least 99% valid pixels for the period of record. To perform the replication analysis, we relaxed the 99% valid pixels criterion to identify an alternative reference year y^*_{alt}. We found that 2007 had 98.5% valid pixels over the Lena delta and 98.7% valid pixels over the Indigirka delta, and therefore chose 2007 as y^*_{alt} for both deltas.

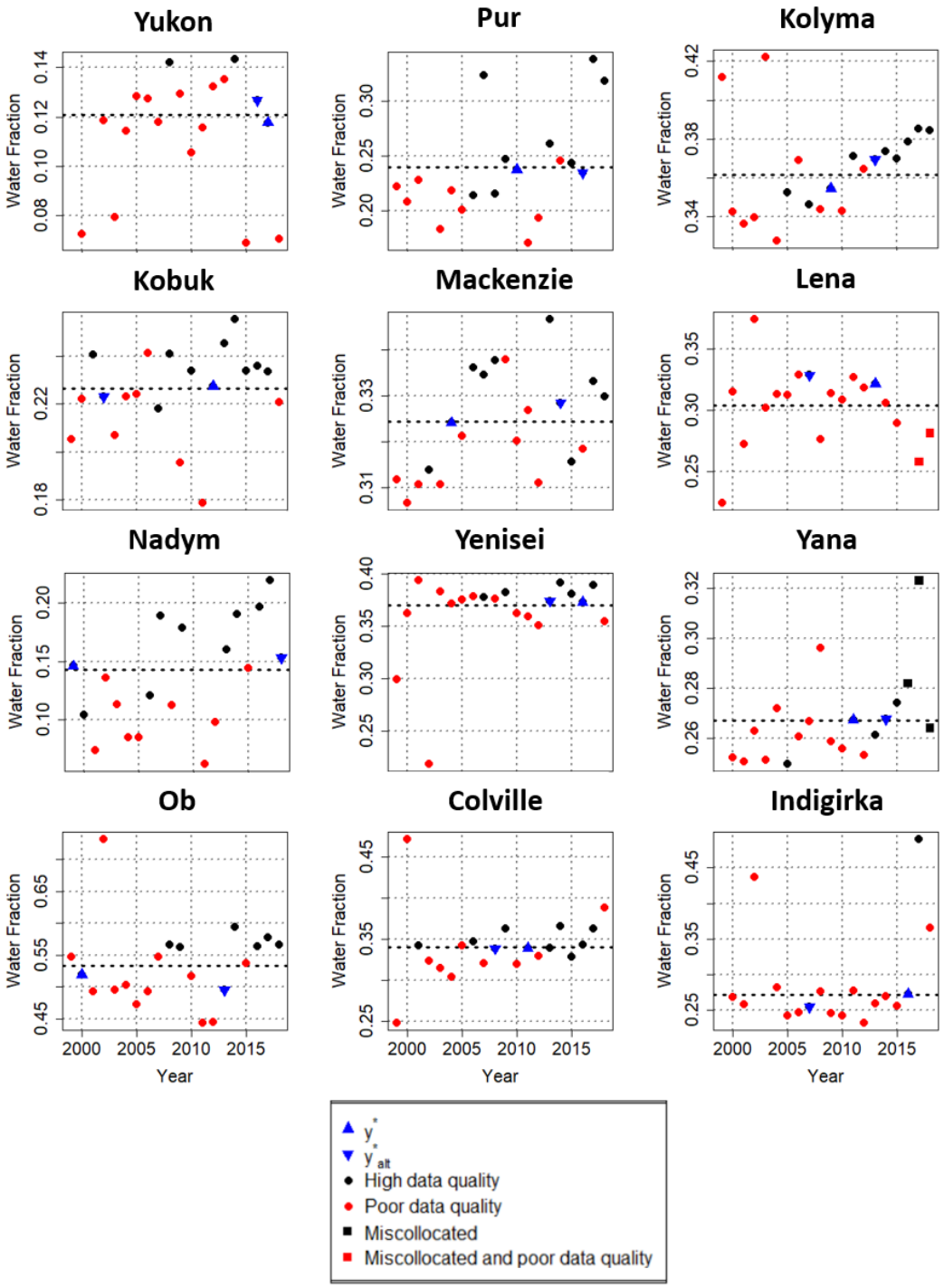

Figure S2. Surface water hydrology of arctic deltas. Time series of July water cover for every delta from 1999 to 2018. Years with at least 99% valid pixels are marked in black and years with less than 99% valid pixels in red, while years chosen for waterbody extraction are in blue triangles. Miscollocated years are shown with squares. The time series of percent valid pixels for each delta is shown in Figure S3.

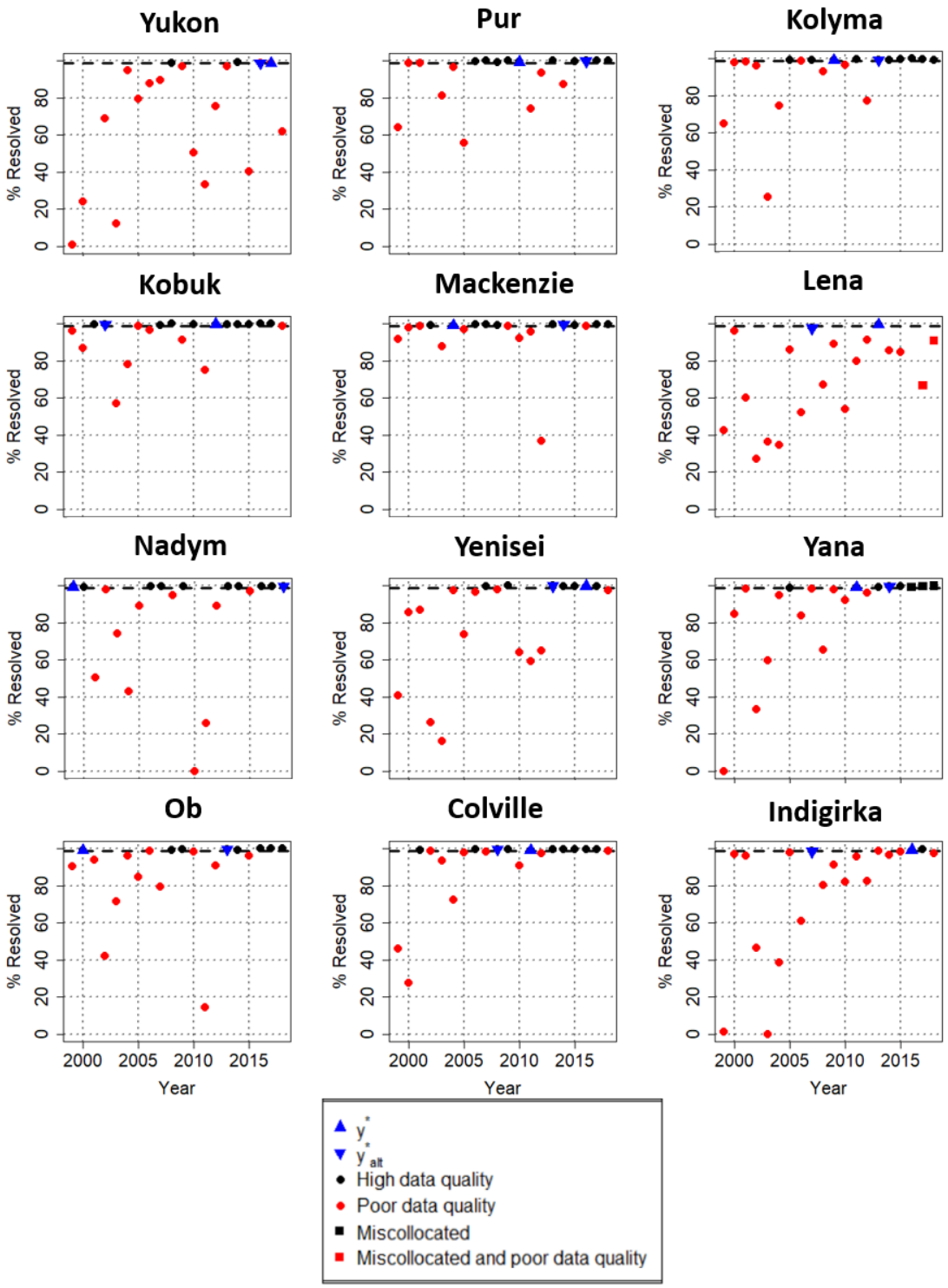

Figure S3. Observational data quality. The percent of pixels resolved in every year on the period of record for the deltas, with symbology the same as in Figure S2.

III. Proportionate growth model

Proportionate growth models, which describe processes where objects grow proportional to their size but the growth is stochastic, have seen widespread applications e.g. in modelling micro-organism sizes, income distribution, and city sizes (Crow & Shimizu, 1989; Mitzenmacher 2004). An interesting property of the proportionate growth models is that they result in a lognormal distribution of the size of the objects, with the parameters related to the parameters of the stochastic growth rate. On the basis that the greater thermal inertia of larger lakes results in lake waters remaining unfrozen for longer and maintaining greater lake to soil temperature gradients, we assume that lake growth is proportional to the size of the lake, which has been observed in Alaska (Jones et al. 2011). Then for a lake with radius r_j at the beginning of a time period j of length Δt, its growth rate $\frac{\Delta r_j}{\Delta t}$ is given by Equation (S1).

$$\frac{\Delta r_j}{\Delta t} = r_j k_j. \tag{S1}$$

We can assume that the proportional growth rate k_j at each timestep is an independent and identically distributed random variable characterized by mean γ and variance φ^2, reflecting the variability in water and soil temperature, precipitation, and soil ice content and matrix properties all of which impact lateral heat fluxes. It is easy to show from Equation (S1) that the distribution of the lake radii after some time period t (arising as the sum of the initial lake radius and its subsequent incremental growths Δr_j over the cumulative period of time) will approach a lognormal distribution (31), i.e., $\ln(r) \sim N(\gamma t, \varphi^2 t)$ (see Equation 1 with no lower bound). Assuming a circular shape of the lake it follows that $\ln(A) = \ln(\pi r^2) \sim N(2\gamma t + \ln(\pi), 4\varphi^2 t) = N(\nu, \beta^2)$, i.e. lake areas are also lognormally distributed with parameters, ν and β^2, and similarly for the volume. A similar model was proposed by Victorov et al. (2019) for thermokarst lakes although empirical testing did not reveal ubiquity of the lognormal size distribution likely due to the mixing of lakes and wetlands in the studied domains.

IV. Fitted distribution parameters and climate trends for lakes, wetlands, and waterbodies

This section contains tables and plots of the fitted distributions and climate trends for lakes, wetlands, and all waterbodies in the reference and alternative reference years. The fitted distribution parameters of lakes and wetlands for a range of waterbody occurrence index thresholds θ used to classify waterbodies extracted in y^* are in Tables (S1 to S3), lake and wetland distribution properties for waterbodies extracted in an alternative reference year y^*_{alt} in Table (S4), the fitted lognormal distribution parameters for waterbody sizes extracted in y^* in Table (S5), the plots of fitted distributions and climate trends of lakes and wetlands extracted in y^*_{alt} (Figures S4 and S5), fitted distributions and climate trends of waterbody sizes extracted in y^* (Figure S6) and boxplots of the waterbody, wetland, and lake size distributions extracted in y^* in Figure (S7).

Table S1. Properties of lake and wetland size distributions at occurrence index threshold θ = 0.85. For each delta, the fitted lognormal parameters ν and β, and number of lakes, N_{Lake}, and p-value (p_{lake}) from a Lilliefors-corrected Kolmogorov Smirnov test (KS test), as well as the fitted power law exponent α, fitted minimum lake size x_0, observed maximum wetland size A_{max}, the number of wetlands $N_{wetland}$ in the range [x_0, A_{max}], and p-value ($p_{Wetland}$) from a KS test. We report the parameters ν and β in $\log_{10}$ scale rather than in Napierian logarithmic scale (ln) as they are easier to interpret. The fitted distributions which cannot be rejected at the 5% significance level **(p > 0.05) are bolded**.

Delta	N_{Lake}	ν [-]	β [-]	p_{Lake}	$N_{Wetland}$ (above x_0)	x_0 [10^5 m^2]	A_{max} [10^5 m^2]	α [-]	$p_{Wetland}$
Yukon	1,511	3.87	0.80	**0.278**	401	0.135	2.835	2.55	**0.052**
Kobuk	1,272	4.40	0.82	**0.688**	196	0.09	3.924	2.30	**0.105**
Nadym	866	4.46	0.70	**0.404**	1,005	0.144	52.092	1.91	**0.143**
Ob	1,567	4.32	0.82	**0.843**	940	0.054	31.428	1.77	**0.306**
Pur	2,407	4.24	0.75	0.008	556	0.117	21.411	1.81	**0.289**
Mackenzie	20,318	4.37	0.75	0.025	1,404	0.189	30.168	2.39	**0.636**
Yenisei	4,058	4.62	0.60	0.038	1,028	0.153	10.620	2.47	0.049
Colville	338	4.57	0.79	**0.326**	105	0.162	7.731	2.30	**0.532**
Kolyma	3,084	4.19	0.82	**0.283**	555	0.135	14.202	2.29	**0.576**
Lena	11,265	4.49	0.74	0.008	1,353	0.477	27.783	2.63	**0.253**
Yana	10,297	4.21	0.88	**0.403**	1,563	0.144	37.872	2.07	**0.511**
Indigirka	4,875	3.91	1.08	**0.162**	1,830	0.099	42.930	1.91	**0.540**

Table S2. Properties of lake and wetland size distributions at occurrence index threshold θ = 0.80. Same as Table S1 but with waterbody classification threshold θ = 0.8. Bolded p-values refer to distributions which cannot be rejected at the 5% significance level.

Delta	N_{Lake}	ν [-]	β [-]	p_{lake}	$N_{Wetland}$ (above x_0)	x_0 [10^5 m^2]	A_{max} [10^5 m^2]	α [-]	$p_{wetland}$
Yukon	1,829	3.80	0.79	**0.137**	252	0.126	1.863	2.74	**0.117**
Kobuk	1,417	4.22	0.87	**0.663**	185	0.054	3.924	2.22	**0.709**
Nadym	1,311	4.31	0.73	**0.645**	1,452	0.063	42.876	1.89	0.019
Ob	1,773	4.17	0.88	**0.825**	734	0.054	21.483	1.82	**0.298**
Pur	2,796	4.07	0.81	**0.168**	784	0.054	21.411	1.85	0.001
Mackenzie	22,495	4.24	0.79	0.016	1,019	0.153	19.620	2.37	**0.824**
Yenisei	4,889	4.50	0.62	0.023	765	0.126	9.090	2.65	**0.773**
Colville	407	4.38	0.84	**0.215**	109	0.108	7.731	2.22	**0.720**
Kolyma	3,613	3.98	0.87	**0.435**	692	0.072	14.202	2.31	**0.995**
Lena	14,156	4.35	0.76	0.047	637	0.540	19.008	2.63	**0.481**
Yana	11,567	4.08	0.91	**0.756**	2,015	0.072	12.789	2.10	**0.251**
Indigirka	5,440	3.74	1.12	**0.062**	1,433	0.099	25.299	1.91	**0.879**

Table S3. Properties of lake and wetland size distributions at occurrence index threshold θ = 0.9. Same as Table S1 but with waterbody classification threshold θ = 0.9. Bolded p-values refer to distributions which cannot be rejected at the 5% significance level.

Delta	N_{Lake}	ν [-]	β [-]	p_{lake}	$N_{Wetland}$ (above x_0)	x_0 [10^5 m^2]	A_{max} [10^5 m^2]	α [-]	$p_{wetland}$
Yukon	1,118	3.95	0.81	**0.279**	185	0.369	15.993	2.69	**0.985**
Kobuk	1,022	4.62	0.76	**0.827**	100	0.333	4.311	2.76	**0.597**
Nadym	433	4.61	0.71	**0.395**	262	1.008	52.092	2.23	**0.610**
Ob	1,275	4.50	0.75	**0.677**	1,232	0.054	43.704	1.75	**0.641**
Pur	1,753	4.47	0.69	0.025	1,356	0.081	23.697	1.85	**0.816**
Mackenzie	16,395	4.55	0.70	**0.091**	2,941	0.198	30.168	2.30	0.000
Yenisei	2,883	4.76	0.58	**0.625**	497	0.486	10.620	2.73	**0.281**
Colville	248	4.77	0.78	**0.382**	167	0.162	7.731	2.22	**0.255**
Kolyma	2,218	4.42	0.79	**0.730**	352	0.378	14.202	2.37	**0.946**
Lena	7,438	4.67	0.73	0.000	2,369	0.495	27.783	2.43	**0.339**
Yana	8,286	4.34	0.86	0.016	2,806	0.144	37.872	1.96	0.000
Indigirka	3,973	4.06	1.08	**0.264**	1,113	0.270	73.431	1.93	**0.276**

Table S4. Properties of lake and wetland size distributions for waterbody extents identified in a duplicate year. Same as Table S1 but for waterbody extent identified in an alternative reference year, y^*_{alt}, with close to average water cover, and using an occurrence index threshold $\theta = 0.85$. Bolded p-values refer to distributions which cannot be rejected at the 5% significance level.

Delta	N_{Lake}	ν [-]	β [-]	p_{lake}	$N_{Wetland}$ (above x_0)	x_0 [10^5 m^2]	A_{max} [10^5 m^2]	α [-]	$p_{wetland}$
Yukon	1,340	3.90	0.81	**0.767**	961	0.081	3.357	2.10	0.003
Kobuk	1,421	4.28	0.83	**0.302**	196	0.054	2.025	2.25	**0.517**
Nadym	867	4.40	0.72	**0.396**	1,358	0.108	50.175	1.81	0.001
Ob	1,440	4.49	0.78	0.007	361	0.288	8.766	2.45	**0.238**
Pur	2,132	4.58	0.63	0.002	404	0.234	15.867	2.59	**0.106**
Mackenzie	18,256	4.46	0.73	**0.080**	2,084	0.189	28.251	2.41	0.001
Yenisei	4,040	4.62	0.60	**0.072**	344	0.324	8.127	2.84	**0.385**
Colville	441	4.25	0.88	**0.312**	140	0.072	2.934	2.20	**0.687**
Kolyma	2,321	4.38	0.80	**0.511**	988	0.153	15.183	2.10	0.029
Lena	12,467	4.37	0.77	**0.059**	1,633	0.324	48.402	2.34	**0.360**
Yana	10,145	4.31	0.84	**0.331**	2,011	0.126	16.470	2.21	**0.090**
Indigirka	5,892	3.90	1.05	**0.197**	866	0.117	23.193	2.31	**0.052**

Table S5. Lognormal waterbody size distribution parameters. Fitted lognormal parameters ν and β, for the waterbody size distribution in the reference year y^*, the number of waterbodies, $N_{waterbody}$, and KS test p-values ($p_{Waterbody}$) used to evaluate the goodness of fit. Bolded p-values refer to distributions which cannot be rejected at the 5% significance level.

Delta	$N_{Waterbody}$	ν [-]	β [-]	$p_{Waterbody}$
Yukon	2,610	2.97	0.97	**0.350**
Kobuk	1,602	3.92	0.97	**0.130**
Nadym	2,945	3.26	1.01	**0.417**
Ob	2,507	3.51	1.08	0.012
Pur	3,580	3.63	0.95	**0.251**
Mackenzie	25,995	3.96	0.88	0.000
Yenisei	6,981	3.97	0.81	0.005
Colville	606	3.50	1.09	**0.417**
Kolyma	4,557	3.35	1.04	**0.674**
Lena	25,604	3.20	1.06	0.000
Yana	14,283	3.53	1.06	0.000
Indigirka	7,807	2.70	1.36	0.043

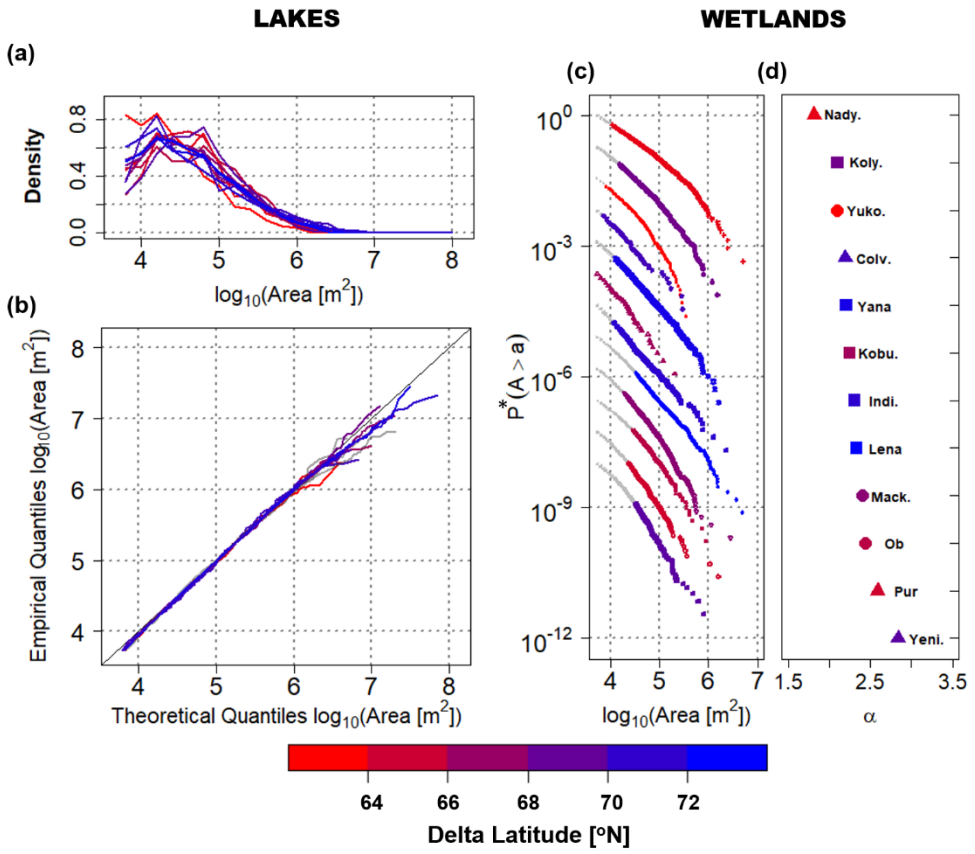

Figure S4. Lake and wetland size distributions extracted in an alternative year. Same as Figure 3 but for waterbody extents identified in an alternative reference year, y^*_{alt}, for all 12 deltas. A truncated lognormal distribution is significant for the lake area distribution at the 5% significance level (KS test) for 10 deltas. The KS test does not reject a power law for the upper tails of the wetland size distributions on 8 out of 12 deltas at a 5% significance level.

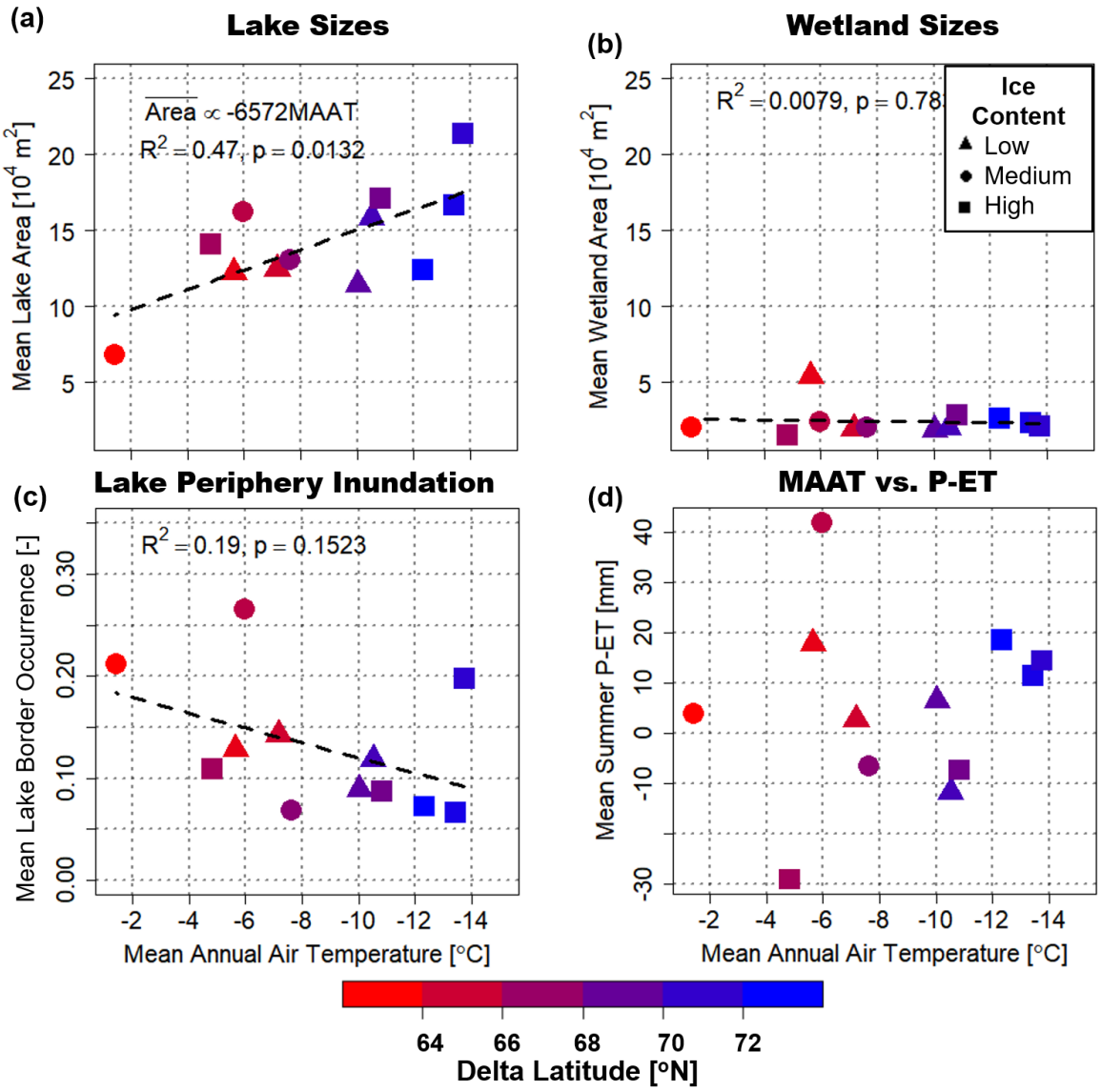

Figure S5. Climate trends for lakes and wetlands extracted in an alternative reference year. (a-c) are the same as Figures 4a, 4b, and 4e, but for waterbody extents identified in an alternative reference year, y^*_{alt}, for all 12 deltas. In (c), the presence of two large outliers (Ob and Indigirka) in (c) renders the trend non-significant. Excluding them to evaluate the relationship among the rest of deltas yields a significant trend (R^2 = 0.66, p = 0.005), supporting a possible relationship. (d) Scatterplot of 2000-2016 mean June to July precipitation minus evapotranspiration (P-ET) over the deltas versus MAAT (27), indicating vertical hydrologic budget is unrelated to differences in MAAT (R^2 = 0.013) and therefore doesn't explain the relationship in (c) or in Figure 4e.

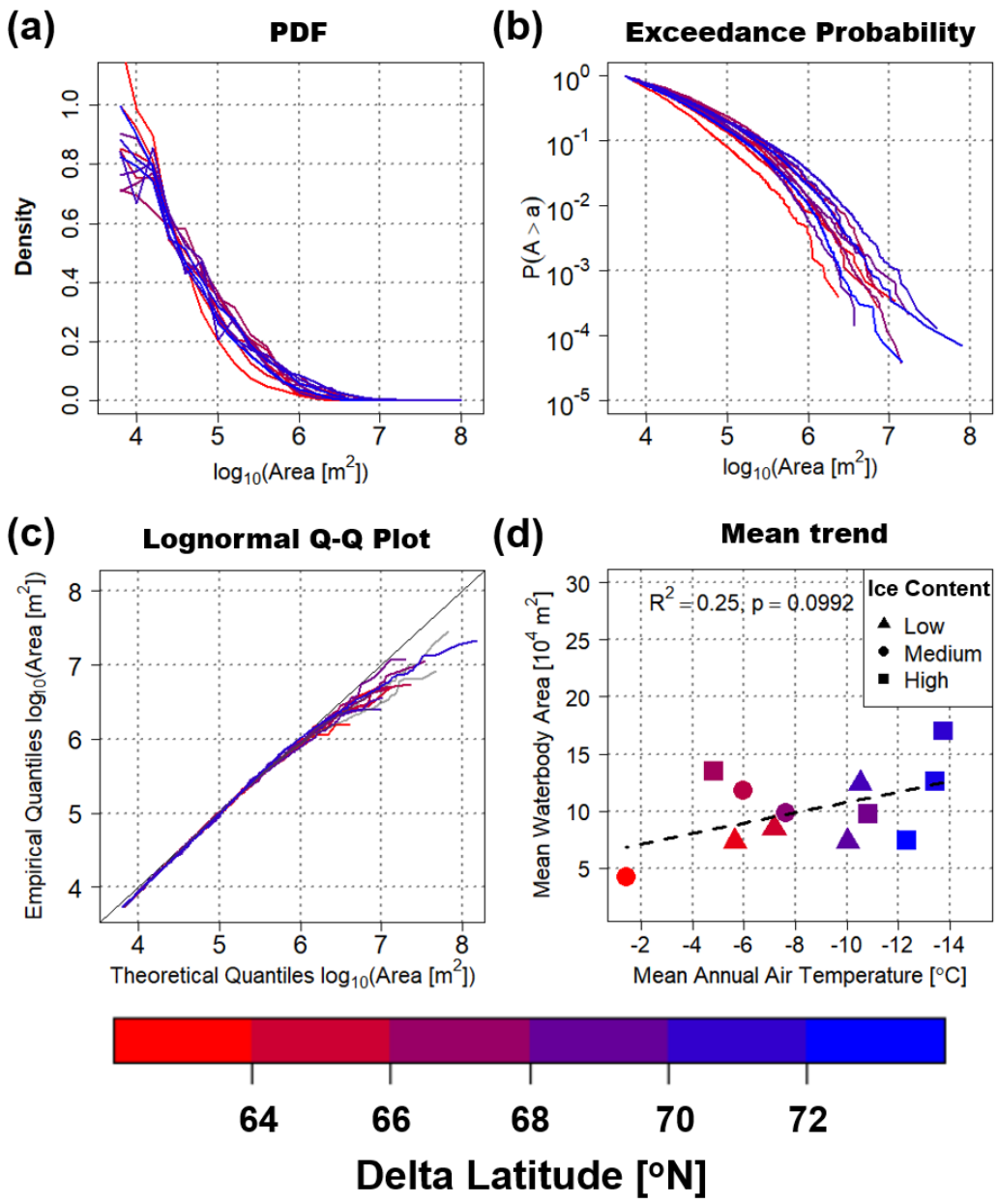

Figure S6. Waterbody size distributions and goodness of fit: (a) The PDF and (b) exceedance probability curves of the waterbody size distributions extracted in the reference year y^*, for all 12 deltas. (c) Q-Q plots of the lognormal distribution fit to the waterbody sizes, for all 12 deltas, with the fitted distributions which are not statistically significant at the 5% significance level (KS test) in grey. (d) Scatterplot of mean waterbody area and MAAT, with delta ice content indicated by point symbol shows no significant linear relationship between the two.

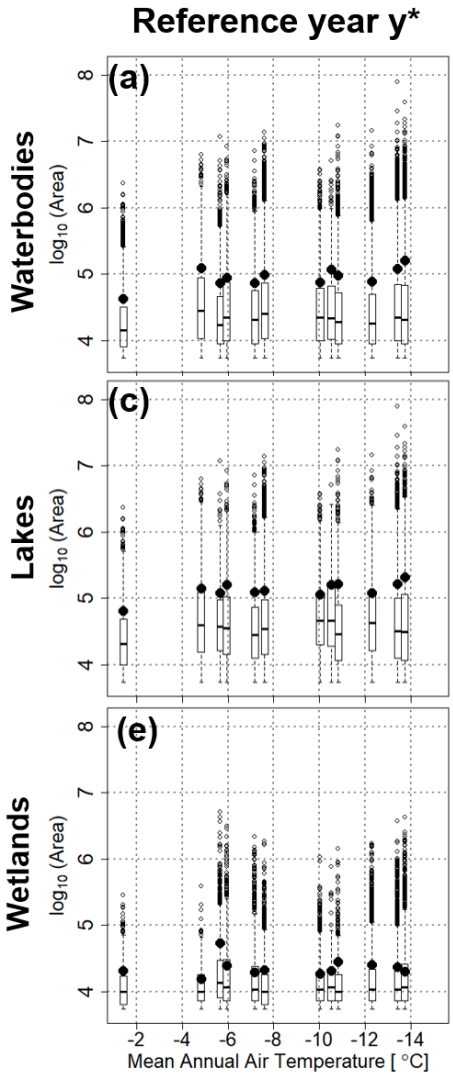

Figure S7. Waterbody, lake, and wetland size distribution boxplots. (a-c) Boxplots of size distribution for all waterbodies (a), lakes (b), and wetlands (c), with boxes representing the interquartile range, whiskers 1.5x the interquartile range, horizontal lines the sample median, and black dots the sample mean. No trend in the median lake size is observed, and a significant trend in the 90th percentile of lake sizes was also found ($p = 0.041$, $R^2 = 0.36$).

V. Relationships between the first three conditional moments

Muster et al. (2019) analyzed 30 regional size distributions of ponds and lakes from the circum-Arctic Permafrost Region Pond and Lake (PeRL) database, and found a linear relationship between the sample mean and the variance, and a hyperbolic relationship between the sample mean and the skewness coefficient of the empirical distributions when estimating these moments over a bounded range, e.g. a lower bound a and an upper bound b, also called the conditional sample moments. They also found that the statistical moments of waterbody sizes identified by inundating a digital elevation model exhibited similar relationships, and therefore determined that pond and lake sizes likely reflect landscape inundation level, rather than reflecting temperature driven growth due to climate. We compared the conditional moments of the 30 PeRL regional size distributions and the lake size distributions on the 12 arctic deltas to investigate if they displayed similar scaling relationships. In Muster et al. (2019) the bounds to compute the conditional sample moments used were $a = 100$ m^2, the minimum reliable lake size from PeRL, and $b = 10^6$ m^2 an upper bound to account for poor sample size for large lakes. We used for both the PeRL regions and the 12 deltas $a = 5.4 \cdot 10^3$ m^2, the minimum reliable lake size estimate in our study and $b = 10^6$ m^2, the same upper bound used in their study. We observed nearly identical relationships between the conditional moments from both data sets (Figure S8). As the relationships between the conditional sample moments of a fitted LN size distribution arising from proportionate growth are indistinguishable from those in the PeRL database, such relationships cannot be used to differentiate between probability distributions and the different mechanisms underlying wetland (inundation) and lake (proportionate growth) formation.

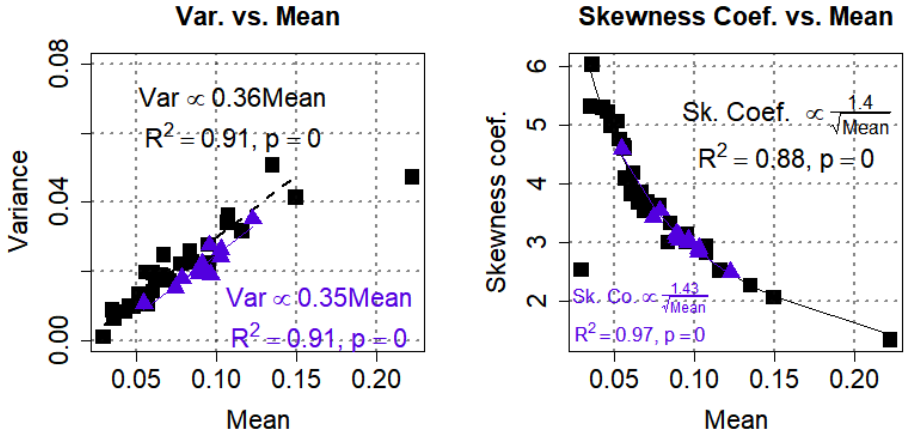

Figure S8. Lake size conditional moment scaling compared with PeRL lake and pond size conditional moment scaling. The conditional mean and conditional variance (a) and the conditional mean and the conditional skewness coefficient (b) of the lakes on arctic deltas (purple triangles) and lakes and ponds examined in Muster et al. (2019) (black squares). The outlier at (0.23 km^2, 0.05 km^4) was discarded to fit the mean and variance relationship (a) and the outlier at (.01 km^2, 2.2) were discarded to fit the mean and skewness relationship (b) for the PeRL data.